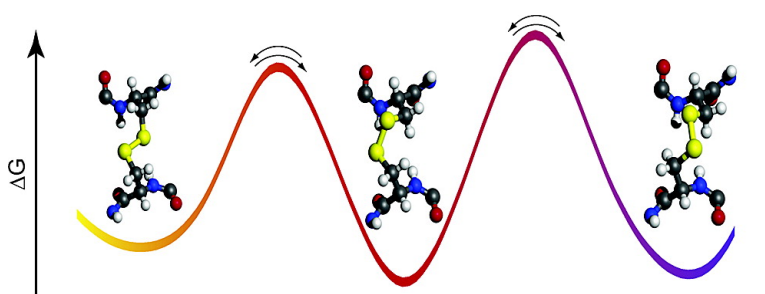**Article**

Disulfide Bond Isomerization in Basic Pancreatic Trypsin Inhibitor: Multisite Chemical Exchange Quantified by CPMG Relaxation Dispersion and Chemical Shift Modeling

Michael J. Grey, Chunyu Wang, and Arthur G. Palmer

More About This Article

Additional resources and features associated with this article are available within the HTML version:

- Supporting Information
- Links to the 12 articles that cite this article, as of the time of this article download
- Access to high resolution figures
- Links to articles and content related to this article
- Copyright permission to reproduce figures and/or text from this article

View the Full Text HTML

Disulfide Bond Isomerization in Basic Pancreatic Trypsin Inhibitor: Multisite Chemical Exchange Quantified by CPMG Relaxation Dispersion and Chemical Shift Modeling

Michael J. Grey, Chunyu Wang, and Arthur G. Palmer, III*

Department of Biochemistry and Molecular Biophysics, Columbia University, 630 West 168th Street, New York, New York 10032

Received June 17, 2003; E-mail: agp6@columbia.edu

Abstract: Conformational changes occurring on the microsecond—millisecond time scale in basic pancreatic trypsin inhibitor (BPTI) are investigated using nuclear magnetic resonance spectroscopy. The rczz CPMG experiment (Wang, C.; Grey, M. J.; Palmer, A. G. *J. Biomol. NMR* **2001**, *21*, 361—366) is used to record ^{15}N spin relaxation dispersion data, $R_{ex}(1/\tau_{cp})$, in which $1/\tau_{cp}$ is the pulsing rate in the CPMG sequence, at two static magnetic fields, 11.7 and 14.1 T, and three temperatures, 280, 290, and 300 K. These data are used to characterize the kinetics and mechanism of chemical exchange line broadening of the backbone ^{15}N spins of Cys 14, Lys 15, Cys 38, and Arg 39 in BPTI. Line broadening is found to result from two processes: the previously identified isomerization of the Cys 38 side chain between χ_1 rotamers (Otting, G.; Liepinsh, E.; Wüthrich, K. *Biochemistry* **1993**, *32*, 3571—3582) and a previously uncharacterized process on a faster time scale. At 300 K, both processes contribute significantly to the relaxation dispersion for Cys 14 and an analytical expression for a linear three-site exchange model is used to analyze the data. At 280 K, isomerization of the Cys 38 side chain is negligibly slow and the faster process dominates the relaxation dispersion for all four spins. Global analysis of the temperature and static field dependence of $R_{ex}(1/\tau_{cp})$ for Cys 14 and Lys 15 is used to determine the activation parameters and chemical shift changes for the previously uncharacterized chemical exchange process. Through an analysis of a database of chemical shifts, ^{15}N chemical shift changes for Cys 14 and Lys 15 are interpreted to result from a χ_1 rotamer transition of Cys 14 that converts the Cys 14—Cys 38 disulfide bond between right- and left-handed conformations. At 290 K, isomerization of Cys 14 occurs with a forward and reverse rate constant of 35 s^{-1} and 2500 s^{-1}, respectively, a time scale more than 30-fold faster than the Cys 38 χ_1 isomerization. A comparison of the kinetics and thermodynamics for the transitions between the two alternative Cys 14—Cys 38 conformations highlights the factors that affect the contribution of disulfide bonds to protein stability.

Introduction

Nuclear magnetic resonance (NMR) spectroscopy is a powerful experimental technique for characterizing dynamic processes that take place on a wide range of time scales in macromolecules. Over the past decade, new NMR spin relaxation methods[1–9] that are sensitive to chemical exchange processes on the microsecond-millisecond time scales have been developed based on the Carr—Purcell—Meiboom—Gill (CPMG)[10,11] and $R_{1\rho}$[12] techniques. These methods have been used to reveal functionally relevant conformational fluctuations in calmodulin,[13–15] HIV protease,[16] L99A T4 lysozyme cavity mutant,[17,18] and cyclophilin A.[19] Both experimental methods and applications have been reviewed recently.[20,21]

Chemical exchange line broadening of nuclear magnetic spin resonances arises from kinetic transitions, between two or more chemical or conformational states of a molecule, that result in time-dependent modulations of isotropic chemical shifts.[22] The effects of chemical exchange are manifested as increased line

(1) Akke, M.; Palmer, A. G. *J. Am. Chem. Soc.* **1996**, *118*, 911—912.
(2) Ishima, R.; Wingfield, P. T.; Stahl, S. J.; Kaufman, J. D.; Torchia, D. A. *J. Am. Chem. Soc.* **1998**, *120*, 10 534—10 542.
(3) Loria, J. P.; Rance, M.; Palmer, A. G. *J. Am. Chem. Soc.* **1999**, *121*, 2331—2332.
(4) Ishima, R.; Louis, J. M.; Torchia, D. A. *J. Am. Chem. Soc.* **1999**, *121*, 11 589—11 590.
(5) Millet, O.; Loria, J. P.; Kroenke, C. D.; Pons, M.; Palmer, A. G. *J. Am. Chem. Soc.* **2000**, *122*, 2867—2877.
(6) Mulder, F. A. A.; Skrynnikov, N. R.; Hon, B.; Dahlquist, F. W.; Kay, L. E. *J. Am. Chem. Soc.* **2001**, *123*, 967—975.
(7) Skrynnikov, N. R.; Mulder, F. A. A.; Hon, B.; Dahlquist, F. W.; Kay, L. E. *J. Am. Chem. Soc.* **2001**, *123*, 4556—4566.
(8) Mulder, F. A. A.; Hon, B.; Mittermaier, A.; Dahlquist, F. W.; Kay, L. E. *J. Am. Chem. Soc.* **2002**, *124*, 1443—1451.
(9) Ishima, R.; Torchia, D. A. *J. Biomol. NMR* **2003**, *25*, 243—248.
(10) Carr, H. Y.; Purcell, E. M. *Phys. Rev.* **1954**, *94*, 630—638.
(11) Meiboom, S.; Gill, D. *Rev. Sci. Instrum.* **1958**, *29*, 688—691.

(12) Deverell, C.; Morgan, R. E.; Strange, J. H. *Mol. Phys.* **1970**, *18*, 553—559.
(13) Evenäs, J.; Forsén, S.; Malmendal, A.; Akke, M. *J. Mol. Biol.* **1999**, *289*, 603—617.
(14) Evenäs, J.; Malmendal, A.; Akke, M. *Structure* **2001**, *9*, 185—195.
(15) Malmendal, A.; Evenäs, J.; Forsén, S.; Akke, M. *J. Mol. Biol.* **1999**, *293*, 883—899.
(16) Ishima, R.; Freedberg, D. I.; Wang, Y.-X.; Louis, J. M.; Torchia, D. A. *Structure* **1999**, *7*, 1047—1055.
(17) Mulder, F. A. A.; Hon, B.; Muhandiram, D. R.; Dahlquist, F. W.; Kay, L. E. *Biochemistry* **2000**, *39*, 12 614—12 622.
(18) Mulder, F. A. A.; Mittermaier, A.; Hon, B.; Dahlquist, F. W.; Kay, L. E. *Nat. Struct. Biol.* **2001**, *8*, 932—935.
(19) Eisenmesser, E. Z.; Bosco, D. A.; Akke, M.; Kern, D. *Science* **2002**, *295*, 1520—1523.
(20) Palmer, A. G.; Kroenke, C. D.; Loria, J. P. *Methods Enzymol.* **2001**, *339*, 204—238.
(21) Akke, M. *Curr. Opin. Struct. Biol.* **2002**, *12*, 642—647.

widths or, equivalently, transverse relaxation rate constants. The kinetic rate constants, site populations, and chemical shift changes describing the exchange process can be determined by measuring the dependence of relaxation rate constants on the pulsing rate in CPMG experiments or the applied radio frequency field strength in $R_{1\rho}$ experiments.[20] The effective field dependence of relaxation rate constants is commonly termed relaxation dispersion.

Spin relaxation dispersion is analyzed by invoking a model for the kinetic process and optimizing the parameters of the model against the experimental data. Relatively simple analytical expressions exist for both CPMG[23-28] and $R_{1\rho}$[12,29,30] experiments assuming a two-site kinetic model. Accordingly, relaxation dispersion data for proteins, including the aforementioned applications, have been analyzed assuming that a two-site model is appropriate, even though more complex kinetic schemes are to be expected. For example, cluster analysis of chemical exchange rate constants,[14] dependence of chemical exchange on ligand concentration,[19] and anomalous curve-fitting results[28,31] all suggest that more than two states are populated and contribute to chemical exchange broadening in particular instances.

Establishing the mechanisms of chemical exchange phenomena in proteins is facilitated if the fitted kinetic rate constants can be correlated with rate constants for ligand binding[14,18,19] and catalysis[19,32,33] or if the fitted chemical shift changes can be correlated with structural changes observed for different functional states, such as apo and ligand-bound conformations.[14] However, independent information about kinetic mechanisms and alternative structural states is not available a priori in all circumstances; indeed, such information can never be available for truly novel dynamic processes.[34] In some cases, relatively simple relationships, such as the scaling between ^{15}N and ^{1}H exchange broadening[16] or the dependence of chemical shifts on secondary structure,[31,35,36] have been used to obtain some information about alternative conformational states.

This paper describes novel approaches for analyzing and interpreting relaxation dispersion data to characterize the kinetic, thermodynamic, and structural basis for chemical exchange phenomena in proteins, using basic pancreatic trypsin inhibitor (BPTI) as an example. Kinetic processes on microsecond-millisecond time scales in BPTI (Figure 1) have been investigated extensively by NMR spectroscopy, including 180° aromatic ring flips,[37,38] exchange of the buried water molecule
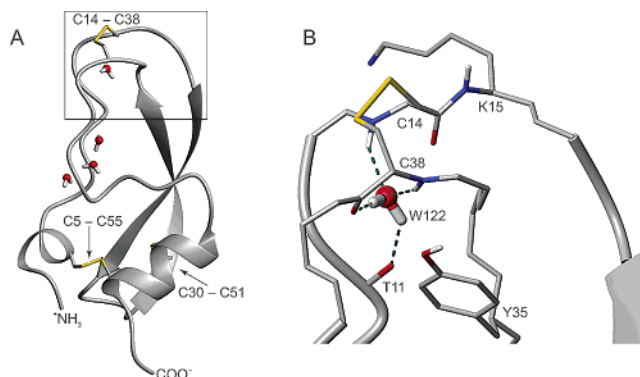

Figure 1. Structure of BPTI. (A) Backbone ribbon diagram representing the overall fold of BPTI in crystal form II drawn from PDB file 5pti.[52] The boxed region is shown as an expansion in (B). The three disulfide bonds are indicated in gold, and the four structurally conserved water molecules are depicted using ball-and-stick representations. The C14−C38 disulfide bond covalently links the two loops comprising the trypsin binding interface. This disulfide is shown in the major conformation (*M*) discussed in the text, with C14 and C38 χ_1 dihedral angles of −60° and +60°, respectively. The figure was drawn using MOLMOL.[82]

Wat 122 with bulk solvent,[39] and isomerization of the C14−C38 disulfide bond resulting from rotation of the C38 χ_1 dihedral angle from +60° to −60°.[5,40,41] Szyperski et al.[41] used on-resonance $R_{1\rho}$ experiments to identify an additional chemical exchange process affecting C14 and K15. However, experimental limitations prevented determination of the kinetic rate constants and mechanism of this exchange process. In the present work, line broadening of the backbone ^{15}N spins of residues C14, K15, C38, and R39 in BPTI have been reinvestigated using the rczz CPMG experiment,[42] a modified version of the rc CPMG experiment[3] with enhanced sensitivity to chemical exchange, to elucidate the nature of the previously uncharacterized motional mode in the vicinity of the C14−C38 disulfide bond.

A global analysis of the relaxation dispersion data collected at static magnetic fields of 11.7 and 14.1 T and temperatures of 280, 290, and 300 K demonstrates that the line broadening of these residues results from both the known isomerization of the C38 χ_1 dihedral angle and an additional process on a faster time scale. The chemical shift changes for the conformation populated by the second kinetic process are found to be consistent with the isomerization of the C14 χ_1 dihedral angle from −60° to +60° by comparisons with chemical shifts in a uniformly referenced chemical shift database[43] and chemical shifts calculated for model conformations.[44] Thus, the C14−C38 disulfide bond has an additional, previously unsuspected, conformation that is characterized by the rotation of the C14 χ_1 dihedral angle from −60° to +60°. At 300 K, both C14 and C38 χ_1 dihedral angle transitions contribute to the exchange line broadening of C14 and an analytical expression describing fast-limit chemical exchange in a linear three-site kinetic model is required to fit the dispersion data. At 290 K, the isomerization

(22) Cavanagh, J.; Fairbrother, W. J.; Palmer, A. G.; Skelton, N. J. *Protein NMR Spectroscopy: Principles and Practice*; Academic Press: San Diego, 1996.
(23) Luz, Z.; Meiboom, S. *J. Chem. Phys.* **1963**, *39*, 366−370.
(24) Carver, J. P.; Richards, R. E. *J. Magn. Reson.* **1972**, *6*, 89−105.
(25) Jen, J. *J. Magn. Reson.* **1978**, *30*, 111−128.
(26) Davis, D. G.; Perlman, M. E.; London, R. E. *J. Magn. Reson., Ser. B* **1994**, *104*, 266−275.
(27) Ishima, R.; Torchia, D. A. *J. Biomol. NMR* **1999**, *14*, 369−372.
(28) Tollinger, M.; Skrynnikov, N. R.; Mulder, F. A. A.; Forman-Kay, J. D.; Kay, L. E. *J. Am. Chem. Soc.* **2001**, *123*, 11 341−11 352.
(29) Meiboom, S. *J. Chem. Phys.* **1961**, *34*, 375−388.
(30) Trott, O.; Abergel, D.; Palmer, A. G. *Mol. Phys.* **2003**, *101*, 753−763.
(31) Hill, R. B.; Bracken, C.; DeGrado, W. F.; Palmer, A. G. *J. Am. Chem. Soc.* **2000**, *122*, 11 610−11 619.
(32) Rozovsky, S.; Jogl, G.; Tong, L.; McDermott, A. E. *J. Mol. Biol.* **2001**, *310*, 271−280.
(33) Cole, R.; Loria, J. P. *Biochemistry* **2002**, *41*, 6072−6081.
(34) Vugmeyster, L.; Kroenke, C. D.; Picart, F.; Palmer, A. G.; Raleigh, D. P. *J. Am. Chem. Soc.* **2000**, *122*, 5387−5388.
(35) Skrynnikov, N. R.; Dahlquist, F. W.; Kay, L. E. *J. Am. Chem. Soc.* **2002**, *124*, 12 352−12 360.
(36) Wagner, G.; DeMarco, A.; Wüthrich, K. *Biophys. Struct. Mech.* **1976**, *2*, 139−158.
(38) Wagner, G.; Wüthrich, K. *Nature* **1978**, *275*, 247−248.
(39) Denisov, V. P.; Peters, J.; Hörlein, H. D.; Halle, B. *Nat. Struct. Biol.* **1996**, *3*, 505−509.
(40) Otting, G.; Liepinsh, E.; Wüthrich, K. *Biochemistry* **1993**, *32*, 3571−3582.
(41) Szyperski, T.; Luginbuehl, P.; Otting, G.; Guentert, P.; Wüthrich, K. *J. Biomol. NMR* **1993**, *3*, 151−164.
(42) Wang, C.; Grey, M. J.; Palmer, A. G. *J. Biomol. NMR* **2001**, *21*, 361−366.
(43) Zhang, H.; Neal, S.; Wishart, D. S. *J. Biomol. NMR* **2003**, *25*, 173−195.
(44) Neal, S.; Nip, A. M.; Zhang, H.; Wishart, D. S. *J. Biomol. NMR* **2003**, *26*, 215−240.

of the C14 χ_1 dihedral angle is more than 30-fold faster than isomerization of the C38 χ_1 dihedral angle, and the conformation of BPTI with the C14 χ_1 dihedral angle of $+60°$ has an equilibrium population of 1.4%, approximately 2-fold lower than the conformation of BPTI with C38 χ_1 of $-60°$. The differences in the kinetics and thermodynamics of the two C14−C38 isomerization reactions highlight the contributions of disulfide bonds to protein stability.

The results of the present investigation demonstrate that multisite exchange phenomena in proteins can be characterized by relaxation dispersion methods, and that novel kinetic processes and conformational states can be identified by modeling chemical shift changes extracted from relaxation dispersion data. The methods utilized herein promise to extend the range of applicability of CPMG and $R_{1\rho}$ spin relaxation dispersion techniques for characterizing dynamic processes in proteins and other biological macromolecules.

Theory

Under conditions for which the evolution of magnetization in a CPMG experiment[10,11] is dominated by a single-exponential decay term, the transverse relaxation rate constant for a single spin exchanging between N sites is given by[45]

$$R_2(1/\tau_{cp}) = R_2^0 - \frac{1}{2\tau_{cp}}\ln \lambda \qquad (1)$$

in which τ_{cp} is the delay between 180° pulses in the CPMG pulse train; λ is the largest eigenvalue of the Hermetian matrix $\mathbf{L}$

$$\mathbf{L} = \exp(\mathbf{A}^\dagger \tau_{cp}) \exp(\mathbf{A}\tau_{cp}) \qquad (2)$$

where $\mathbf{A} = \mathbf{K}' + \rho + i\omega$; $\mathbf{K}' = \mathbf{S}^{-1}\mathbf{K}\mathbf{S}$ is a symmetric matrix; and $\mathbf{K}$ is the chemical kinetic rate matrix with elements

$$K_{ij} = k_{ji} \ (i \neq j)$$

$$K_{ii} = -\sum_{\substack{j=1 \\ j \neq i}}^{N} k_{ij} \qquad (3)$$

where ρ is a diagonal matrix with elements $\rho_{ij} = \delta_{ij} (R_{2i} - R_2^0)$; δ_{ij} is the Kroenecker delta function; ω is a diagonal matrix with elements $\omega_{ij} = \delta_{ij} \Omega_i$; $\mathbf{S}$ is a diagonal matrix with elements $S_{ij} = \delta_{ij} p_i^{1/2}$; R_{2i} is the transverse relaxation rate constant for a spin in the ith site in the absence of chemical exchange effects, arising from dipole−dipole (DD) and chemical shift anisotropy (CSA) interactions; R_2^0 is the population-average transverse relaxation rate constant in the absence of chemical exchange effects; Ω_i is the resonance offset in the rotating frame for a spin in the ith site; p_i is the population of the ith site; and k_{ij} is the first-order rate constant for transitions from site i to site j. Differences between DD and CSA relaxation rate constants for different sites can be neglected if $\rho_{ii} \ll K_{ii}$; this assumption is made in the following. Thus, the chemical exchange contribution to transverse relaxation is defined by

$$R_{ex}(1/\tau_{cp}) = -\frac{1}{2\tau_{cp}}\ln \lambda \qquad (4)$$

(45) Allerhand, A.; Thiele, E. *J. Chem. Phys.* **1966**, *45*, 902−916.

If necessary, the expressions given below can be modified to incorporate the effects of site-to-site differences in R_{2i} by redefining $K_{ii} \rightarrow K_{ii} + \rho_{ii}$.

In the limit of fast exchange, in which a single population−average resonance signal is observed with frequency $\bar{\Omega}$[45]

$$R_{ex}(1/\tau_{cp}) = \sum_{n=2}^{N} \frac{\langle u_1|\omega|u_n\rangle^2}{\kappa_n}\left(1 - \frac{2 \tanh [\kappa_n\tau_{cp}/2]}{\kappa_n\tau_{cp}}\right) \qquad (5)$$

in which κ_n is the absolute value of the nth eigenvalue and u_n is the nth eigenvector of $\mathbf{K}'$, respectively. In the presence of a strong effective field, i.e., infinitely fast pulsing, $R_{ex}(1/\tau_{cp} \rightarrow \infty) \rightarrow 0$. In the absence of an applied field, i.e., $1/\tau_{cp} \rightarrow 0$, the maximal free-precession exchange contribution, $R_{ex}(1/\tau_{cp} \rightarrow 0)$, is observed

$$R_{ex}(1/\tau_{cp} \rightarrow 0) = \sum_{n=2}^{N} \frac{\langle u_1|\omega|u_n\rangle^2}{\kappa_n} \qquad (6)$$

For a two-site chemical kinetic process, represented by

$$A \underset{k_{-1}}{\overset{k_1}{\rightleftharpoons}} B \qquad (7)$$

Equation 4 can be solved analytically to give[24]

$$R_{ex}(1/\tau_{cp}) = \frac{1}{2}\left(k_{ex} - \frac{1}{\tau_{cp}}\cosh^{-1}[D_+ \cosh(\eta_+) - D_- \cos(\eta_-)]\right) \qquad (8)$$

where

$$D_\pm = \frac{1}{2}\left[\pm 1 + \frac{\psi + 2\Delta\omega^2}{(\psi^2 + \zeta^2)^{1/2}}\right]^{1/2}$$

$$\eta_\pm = \frac{\tau_{cp}}{\sqrt{2}}[\pm\psi + (\psi^2 + \zeta^2)^{1/2}]^{1/2} \qquad (9)$$

where $\psi = k_{ex}^2 - \Delta\omega^2$, $\zeta = -2\Delta\omega k_{ex} (p_A - p_B)$, $k_{ex} = k_1 + k_{-1}$, and $\Delta\omega = \Omega_B - \Omega_A$. The rate constants and populations are related by $p_A = k_{-1}/k_{ex}$ and $p_B = 1 - p_A$. In the limit of fast exchange, eq 5 can be expressed as[23]

$$R_{ex}(1/\tau_{cp}) = \frac{p_A p_B \Delta\omega^2}{k_{ex}}\left(1 - \frac{2\tanh [\tau_{cp}k_{ex}/2]}{\tau_{cp}k_{ex}}\right) \qquad (10)$$

Assuming that $\Delta\omega$ is independent of temperature, the temperature dependence of $R_{ex}(1/\tau_{cp})$ is determined by the activation enthalpies, $\Delta H^\ddagger_{\pm 1}$, and entropies, $\Delta S^\ddagger_{\pm 1}$, for the forward and reverse exchange reactions through

$$k_{\pm 1}(T) = \frac{k_B T}{h} \exp(-\Delta G^\ddagger_{\pm 1}/RT) \qquad (11)$$

where $\Delta G^\ddagger_{\pm 1} = \Delta H^\ddagger_{\pm 1} - T\Delta S^\ddagger_{\pm 1}$, h, k_B, and R represent the Planck, Boltzmann, and universal gas constants, respectively, and T is the absolute temperature. In addition, $p_B/p_A = \exp(-\Delta G/RT)$, in which ΔG is the free energy difference between the two states.
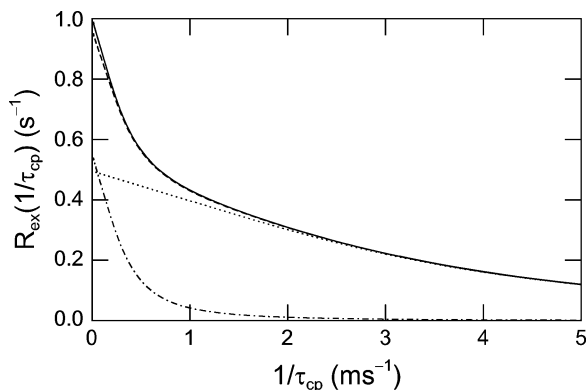
Figure 2. Linear three-site chemical exchange. $R_{ex}(1/\tau_{cp})$ dispersion profiles for chemical exchange between three sites, eq 12, were generated using the fast-limit approximation eq 13 (—) and numerical evaluation of eq 4 (− − −) for (all units of s^{-1}) $k_1 = 10$, $k_{-1} = 1000$, $k_2 = 100$, $k_{-2} = 10\,000$, $\Omega_A = 0$, $\Omega_B = 250$, and $\Omega_C = 750$. The curves are scaled relative to $R_{ex}(1/\tau_{cp} \to 0)$ for eq 13. Also shown are the dispersion profiles for the $A \leftrightarrow B$ (− · − ·) and $A \leftrightarrow C$ (· · · ·) transitions treated with independent two-site exchange models according to eq 10.

For a linear three-site exchange model, represented by

$$C \underset{k_{-2}}{\overset{k_2}{\rightleftharpoons}} A \underset{k_{-1}}{\overset{k_1}{\rightleftharpoons}} B \qquad (12)$$

and arbitrary rate constants, eq 4 must be solved numerically.[28,45] However, in the fast exchange limit, eq 5 can be solved analytically to yield the closed-form expression

$$R_{ex}(1/\tau_{cp}) = \frac{\phi_2}{\kappa_2}\left(1 - \frac{2\tanh[\kappa_2\tau_{cp}/2]}{\kappa_2\tau_{cp}}\right) + \frac{\phi_3}{\kappa_3}\left(1 - \frac{2\tanh[\kappa_3\tau_{cp}/2]}{\kappa_3\tau_{cp}}\right) \qquad (13)$$

in which, $\phi_2 = (-\kappa_3\alpha_1 + \alpha_2)/Z$, $\phi_3 = (-\kappa_2\alpha_1 + \alpha_2)/Z$, $\kappa_2 = (k_{ex} + Z)/2$, $\kappa_3 = (k_{ex} - Z)/2$, and

$$k_{ex} = k_1 + k_{-1} + k_2 + k_{-2}$$

$$Z = (k_{ex}^2 - 4B)^{1/2}$$

$$B = k_{-1}k_{-2} + k_1k_{-2} + k_{-1}k_2$$

$$\alpha_1 = p_Ap_B(\Omega_B - \Omega_A)^2 + p_Bp_C(\Omega_C - \Omega_B)^2 + p_Ap_C(\Omega_C - \Omega_A)^2$$

$$\alpha_2 = p_A[k_1(\Omega_B - \Omega_A)^2 + k_2(\Omega_C - \Omega_A)^2]$$

$$p_A = k_{-1}k_{-2}/B$$

$$p_B = k_1k_{-2}/B$$

$$p_C = k_{-1}k_2/B \qquad (14)$$

To confirm the accuracy of eq 13 and to establish practical guidelines for distinguishing between two- and three-site exchange, $R_{ex}(1/\tau_{cp})$ relaxation dispersion profiles calculated from the fast limit approximation in eq 13 and from the numerical evaluation of eq 4 are compared in Figure 2. When the rates of the two exchange pathways differ by at least an order of magnitude, two distinct dispersion phases are observed, each characterized by a dispersion amplitude, ϕ_i/κ_i, and apparent

exchange rate constant κ_i. Both processes contribute to exchange broadening for weak effective fields, where $1/\tau_{cp}$ is less than κ_i for the slower process. For stronger effective fields, where $1/\tau_{cp}$ is greater than κ_i for the slower process, the dispersion profile is accurately described using the two-state approximation of eq 10 for the faster process.

Longitudinal relaxation in the rotating reference frame provides an alternative approach to CPMG experiments for characterizing chemical exchange.[20] Recently, Abergel and Palmer showed that the rate constant for longitudinal relaxation in the rotating reference frame, $R_{1\rho}$, can be expressed as[46]

$$R_{1\rho} = R_1^0\cos^2\theta + R_2^0\sin^2\theta +$$
$$\sin^2\theta\sum_{n=2}^{N}\frac{\langle u_1|\boldsymbol{\omega}|u_n\rangle^2}{\kappa_n}\left(\frac{\kappa_n^2}{\kappa_n^2 + \omega_e^2}\right) \qquad (15)$$

for N-site chemical exchange in the fast limit, where R_1^0 is the population-average longitudinal relaxation rate constant in the absence of exchange, $\theta = \tan^{-1}(\omega_1/\bar{\Omega})$ is the tilt angle, ω_1 is the amplitude of the B_1 field, and $\omega_e = (\omega_1^2 + \bar{\Omega}^2)^{1/2}$ is the effective field in the rotating frame. The similarity between eq 15 and eqs 1, 4, and 5 demonstrates that an expression for $R_{1\rho}$ for a linear three-site exchange model can be obtained by analogy to eq 13.

Results

Estimating the Chemical Shift Time Scale For Exchange in BPTI. The effects of chemical exchange processes on NMR spectra depend qualitatively on whether exchange is fast ($k_{ex} \gg \Delta\omega$), intermediate ($k_{ex} \approx \Delta\omega$), or slow ($k_{ex} \ll \Delta\omega$) on the chemical shift time scale. The chemical shift time scale can be defined experimentally by the static magnetic field[5] or temperature[47] dependence of $R_{ex}(1/\tau_{cp} \to 0)$. As shown in Figure 3A, as the temperature is decreased, an exchange process changes from fast to intermediate on the chemical shift time scale with a concomitant increase in $R_{ex}(1/\tau_{cp} \to 0)$ to a maximum at the temperature where $k_{ex} = \Delta\omega$. Additional cooling then results in a decrease in $R_{ex}(1/\tau_{cp} \to 0)$ as exchange becomes slow on the chemical shift time scale, to the point where exchange is "frozen out" and no longer contributes to transverse relaxation.

To estimate the chemical shift time scales for exchange processes in BPTI over the temperature range of 280−300 K, $R_{ex}(1/\tau_{cp} \to 0)$, which is difficult to measure directly, was approximated by $R_{ex}(1/\tau_{cp} = 15.4~\text{s}^{-1})$. As shown in Figure 3A, theoretical calculations confirm the accuracy of this approximation. As shown in Figure 3D, $R_{ex}(1/\tau_{cp} = 15.4~\text{s}^{-1}) \approx 0$ for residues in BPTI not subject to exchange broadening. The amide ^{15}N spins of C14 and K15 are subject to a chemical exchange process that is fast on the chemical shift time scale ($k_{ex} \gg \Delta\omega_N$) at 300 and 290 K, and approaches coalescence around 280 K ($k_{ex} = \Delta\omega_N$), as shown in Figure 3B. This behavior is in contrast to that observed for ^{15}N spins of C38 and R39, shown in Figure 3C, where the chemical exchange process resulting from isomerization of the C38 side chain is slow ($k_{ex} \ll \Delta\omega_N$) below 300 K. Assuming large enough chemical shift changes to produce the observed exchange broadening for C14 and K15,

(46) Abergel, D.; Palmer, A. G. *Concepts Magn. Reson.* **2003**, in press.
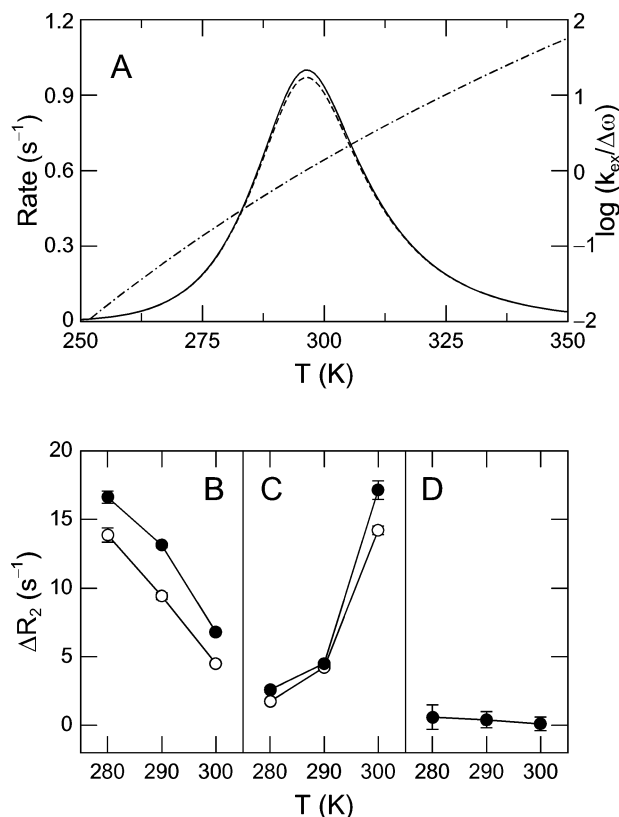(47) Mandel, A. M.; Akke, M.; Palmer, A. G. *Biochemistry* **1996**, *35*, 16 009−16 023.

Figure 3. Temperature dependence of chemical exchange and the chemical shift time scale. (A) The temperature dependence of $R_{ex}(1/\tau_{cp} \rightarrow 0)$ (—) and $\Delta R_2 = R_2^{rczz}(1/\tau_{cp} = 15.4\ s^{-1}) - R_2^{0,rczz}$ (— — —) were simulated for a two-site exchange process using eqs 8 and 11 expressed as a function of temperature for $\Delta H^{\ddagger}_1 = 70$ kJ mol^{-1}, $\Delta S^{\ddagger}_1 = 30$ J mol^{-1} K^{-1}, $\Delta H^{\ddagger}_{-1} = 60$ kJ mol^{-1}, $\Delta S^{\ddagger}_{-1} = 10$ J mol^{-1} K^{-1}, and chemical shift difference $\Delta\omega/2\pi = 100$ Hz. The chemical shift time scale is indicated by $\ln(k_{ex}/\Delta\omega)$ (— · — ·). (B–D) The ^{15}N chemical exchange line broadening was approximated by measuring ΔR_2 at a static magnetic field of 14.1 T and temperatures of 300, 290, and 280 K for (B) C14 (○) and K15 (●), (C) C38 (○) and R39 (●). The average values of ΔR_2 for residues 18–24 and 28–34 in the core β-sheet not subject to chemical exchange are shown in (D).

the underlying dynamic process responsible for exchange broadening is at least an order of magnitude faster than the known isomerization of the C38 side chain.

^{15}N $R_{ex}(1/\tau_{cp})$ Relaxation Dispersion. Initially, relaxation dispersion profiles for C14 and K15 at both 11.7 and 14.1 T static magnetic fields and 300 K were simultaneously analyzed using the fast-limit two-site model, eq 10. However, the two-site chemical exchange model did not adequately reproduce the dispersion data for C14 (not shown). Accordingly, the dispersion data for C14 at 300 K were analyzed using a linear three-site exchange model by simultaneously fitting dispersion data at both fields to eq 13. The data shown in Figure 4 exhibit two dispersion phases, similar to those described in Figure 2, that are characterized by exchange rate constants $\kappa_2 = 220\ s^{-1}$ and $\kappa_3 = 7000\ s^{-1}$. The slower process is consistent with the rate of the C38 side chain isomerization at 300 K.[40] Relaxation dispersion data for K15 were fit nearly equally well by two- and three-site exchange models.

The results presented in Figure 4 demonstrate that effects of the isomerization of the C38 side chain on transverse relaxation of C14 are suppressed when $1/\tau_{cp} \geq 100\ s^{-1}$. The same is true at 290 and 280 K, where the rate of the isomerization is less

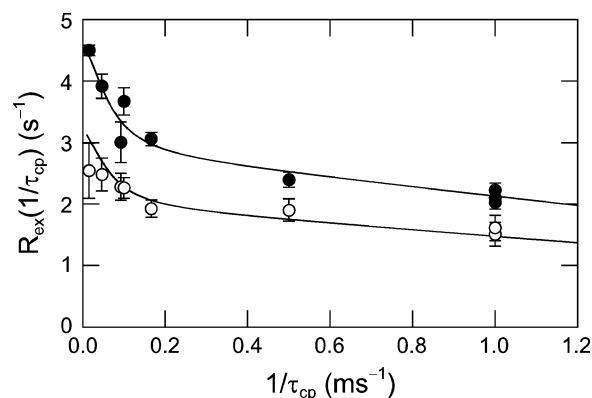**Figure 4.** Chemical exchange at 300 K for C14. ^{15}N $R_{ex}(1/\tau_{cp})$ relaxation dispersion profiles for C14 at 300 K and static magnetic field strengths of 11.7 (○) and 14.1 T (●). The solid lines represent the best simultaneous fit of the data at both static magnetic fields to eq 13 by optimization of ϕ_2, ϕ_3, κ_2, and κ_3.

Table 1. Activation Parameters Derived from Globally Fitting the Temperature Dependence of $R_{ex}(1/\tau_{cp})$ for C14 and K15

	C14	K15	weighted mean
$\Delta H^{\ddagger}_1$ (kJ mol^{-1})	51 ± 7	63 ± 5	59 ± 4
$\Delta S^{\ddagger}_1$ (J mol^{-1} K^{-1})	−40 ± 25	5 ± 17	−13 ± 14
$\Delta H^{\ddagger}_{-1}$ (kJ mol^{-1})	67 ± 4	64 ± 2	65 ± 2
$\Delta S^{\ddagger}_{-1}$ (J mol^{-1} K^{-1})	50 ± 13	40 ± 8	45 ± 7

Table 2. Chemical Exchange Rate Constants and Site Populations for C14 and K15[a]

residue	T (K)	k_1 (s^{-1})	k_{-1} (s^{-1})	p_B (%)
C14	300	55 ± 15	5400 ± 700	1.0 ± 0.2
	290	26 ± 5	2100 ± 200	1.3 ± 0.2
	280	12 ± 2	740 ± 70	1.6 ± 0.1
K15	300	120 ± 20	7400 ± 600	1.5 ± 0.2
	290	47 ± 7	3000 ± 200	1.5 ± 0.2
	280	18 ± 2	1110 ± 90	1.6 ± 0.1

[a] Rate constants and site populations are calculated for each residue based on the activation parameters given in Table 1 and eq 11.

than 100 s^{-1}. Similar conclusions hold for K15 as well. Therefore, by utilizing only dispersion data acquired with $1/\tau_{cp} \geq 100\ s^{-1}$, the faster exchange process affecting C14 and K15 can be treated simply as a two-site exchange process. Results from a global analysis of the dispersion data at three temperatures and two static magnetic field strengths are presented in Figure 5. The data are described well by the two-site chemical exchange model for an activated conformational transition (reduced $\chi^2 = 0.63$ and 0.80 for C14 and K15, respectively). In this model, the amide ^{15}N spins of C14 and K15 occupy two distinct conformations that differ in chemical shift by $|\Delta\omega_N| = 1130 ± 70$ and $1480 ± 80$ s^{-1} (at $B_0 = 11.7$ T), respectively. The activation parameters describing the conformational transition are presented in Table 1. Because similar activation parameters are obtained from the independent analysis of C14 and K15 dispersion data, the ^{15}N spins of these residues appear to be sensing a single kinetic process. Kinetic rate parameters for C14 and K15 are presented in Table 2. Under equilibrium conditions at 290 K, the population of the minor state conformation is $1.4 ± 0.1\%$. This highly skewed population distribution corresponds to a free energy difference between the major and minor state conformations of $\Delta G = 10.3 ± 0.2$ kJ mol^{-1}. The transition to the minor state proceeds with a slightly favorable change in enthalpy ($\Delta H = -7 ± 3$ kJ mol^{-1}) and a significant
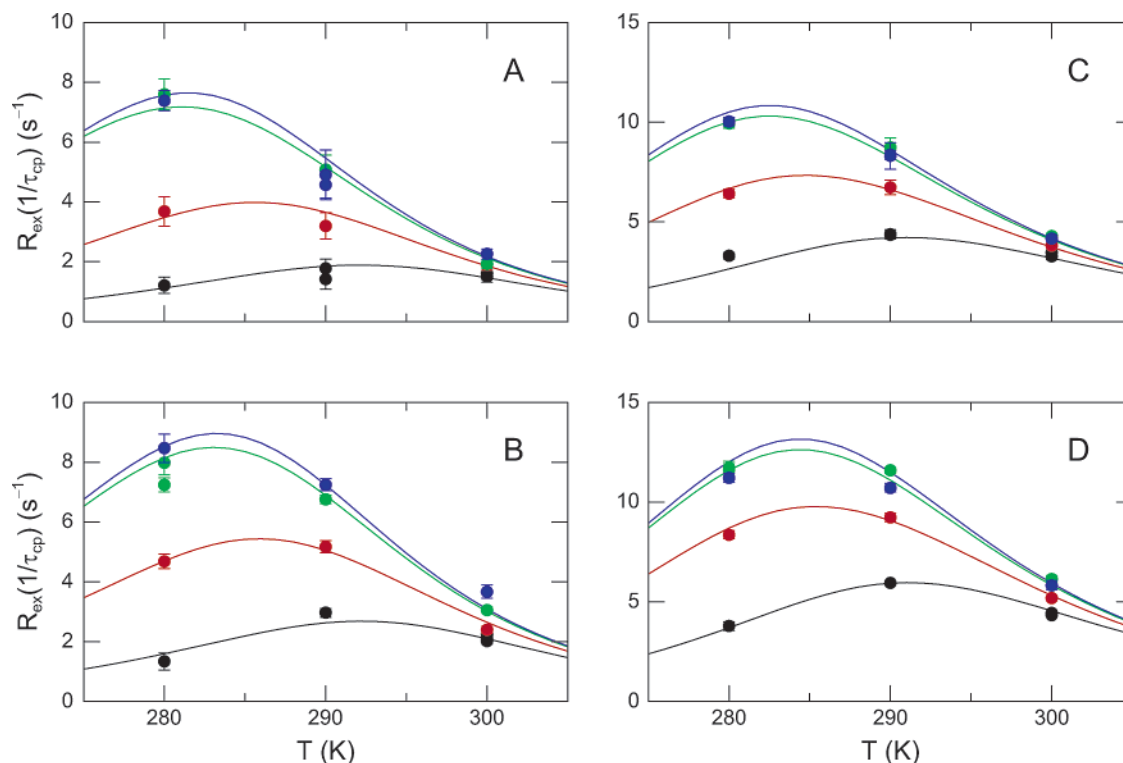
Figure 5. Global analysis of the temperature dependence of chemical exchange for C14 and K15. ^{15}N $R_{ex}(1/\tau_{cp})$ relaxation rate constants for C14 (A, B) and K15 (C, D) at static magnetic field strengths of 11.7 (A, C) and 14.1 T (B, D) and temperatures of 300, 290, and 280 K were measured for $1/\tau_{cp} = 1000$ (black), 500 (red), 166.67 (green) and 100 s^{-1} (blue). The solid lines represent the global fit of the dispersion data at both fields and the three temperatures to eqs 8 and 11 expressed as a function of temperature by optimization of the exchange activation parameters (presented in Table 1) and $\Delta\omega_N$ for each residue.

Table 3. Chemical Exchange Parameters for C38 and R39

residue	T (K)	$\Delta\omega_N$ (s^{-1})[a]	k_{ex} (s^{-1})
C38	300	440 ± 40	580 ± 110
	290	550 ± 100	60 ± 8
	280	270 ± 20^b	730 ± 100
R39	300	1250 ± 60	530 ± 160
	290	1530 ± 70	46 ± 9
	280	380 ± 20^b	1260 ± 120

[a] $\Delta\omega_N$ is reported for a static magnetic field strength of $B_0 = 11.7$ T. [b] $\Delta\omega_N$ at 280 K was determined as $\Delta\omega_N = (R_{ex}k_{ex}/p_Ap_B)^{1/2}$ using the values of p_Ap_B determined for C14 and K15 chemical exchange (Table 2).

unfavorable reduction in entropy, $\Delta S = -60 \pm 10$ J mol^{-1} K^{-1}, that dominates the destabilization of the excited state conformation.

The ^{15}N $R_{ex}(1/\tau_{cp})$ dispersion profiles for C38 and R39 were analyzed separately at each temperature. At 300 and 290 K, the simultaneous fits of the dispersion data at both static fields to eq 8, shown in Figure 6, yielded chemical shift changes and exchange rate constants, shown in Table 3, that are in agreement with the previously determined parameters for the isomerization of the C38 side chain.[5,40,41] At 290 K, the isomerization reaction occurs with an average rate constant of 1 s^{-1}, $\Delta H^{\ddagger} = 55$ kJ mol^{-1}, and $\Delta S^{\ddagger} = -60$ J mol^{-1} K^{-1} for the forward reaction, and an average rate constant of 40 s^{-1}, $\Delta H^{\ddagger} = 45$ kJ mol^{-1}, and $\Delta S^{\ddagger} = -80$ J mol^{-1} K^{-1} for the reverse reaction. At 280 K, this process is too slow, $k_{ex} \approx 25$ s^{-1}, to produce significant exchange contributions to the relaxation of C38 and R39. Instead, $R_{ex}(1/\tau_{cp})$ dispersion profiles are observed that are consistent with fast exchange on the chemical shift time scale. Using the fast limit approximation of eq 10, an average exchange

rate constant of $k_{ex} = 950 \pm 80$ s^{-1} is obtained for C38 and R39, respectively, that agrees well with $k_{ex} = 900 \pm 50$ s^{-1} obtained for C14 and K15 at 280 K. Thus, at 280 K, the exchange contributions to transverse relaxation of the ^{15}N spins of C38 and R39 result from the same fast chemical exchange process that affects C14 and K15. Using the site populations determined for C14 and K15, the faster exchange process results in ^{15}N chemical shift changes of $|\Delta\omega_N| = 270$ and 380 s^{-1} (at $B_0 = 11.7$ T) for C38 and R39, respectively. These values of $\Delta\omega_N$ are much smaller than those observed for the χ_1 isomerization of the C38 side chain previously measured to be 540 and 1180 s^{-1} (at $B_0 = 11.7$ T) for C38 and R39, respectively,[5,40] which suggests that a unique line broadening process is being observed at 280 K. In addition, these values are much smaller than the values of $|\Delta\omega_N| = 1130 \pm 70$ and 1480 ± 80 s^{-1} (at $B_0 = 11.7$ T) observed for C14 and K15 and suggest that the faster kinetic process results in greater conformational perturbations in the vicinity of C14 than C38.

Determining the Sign of $\Delta\omega_N$. As shown by eqs 5, 8, and 15, chemical exchange line broadening depends only on the absolute magnitude of $\Delta\omega_N$. The sign of $\Delta\omega_N$ can be determined, provided that the exchange process is outside the fast exchange limit, because the observed amide ^{1}H$-^{15}$N resonance is shifted closer to the Larmor frequency of the minor state in an HSQC spectrum than in an HMQC spectrum.[36] Values of the resonance frequency difference between the HSQC and HMQC spectra, Ω_N, for the backbone amide ^{15}N spins of BPTI at a static magnetic field of 11.7 T and a temperature of 280 K are shown in Figure 7. The measured values of $\Omega_N/2\pi = -1.0$ and -1.4 Hz for C14 and K15, respectively, indicate that $\Delta\omega_N$ is negative

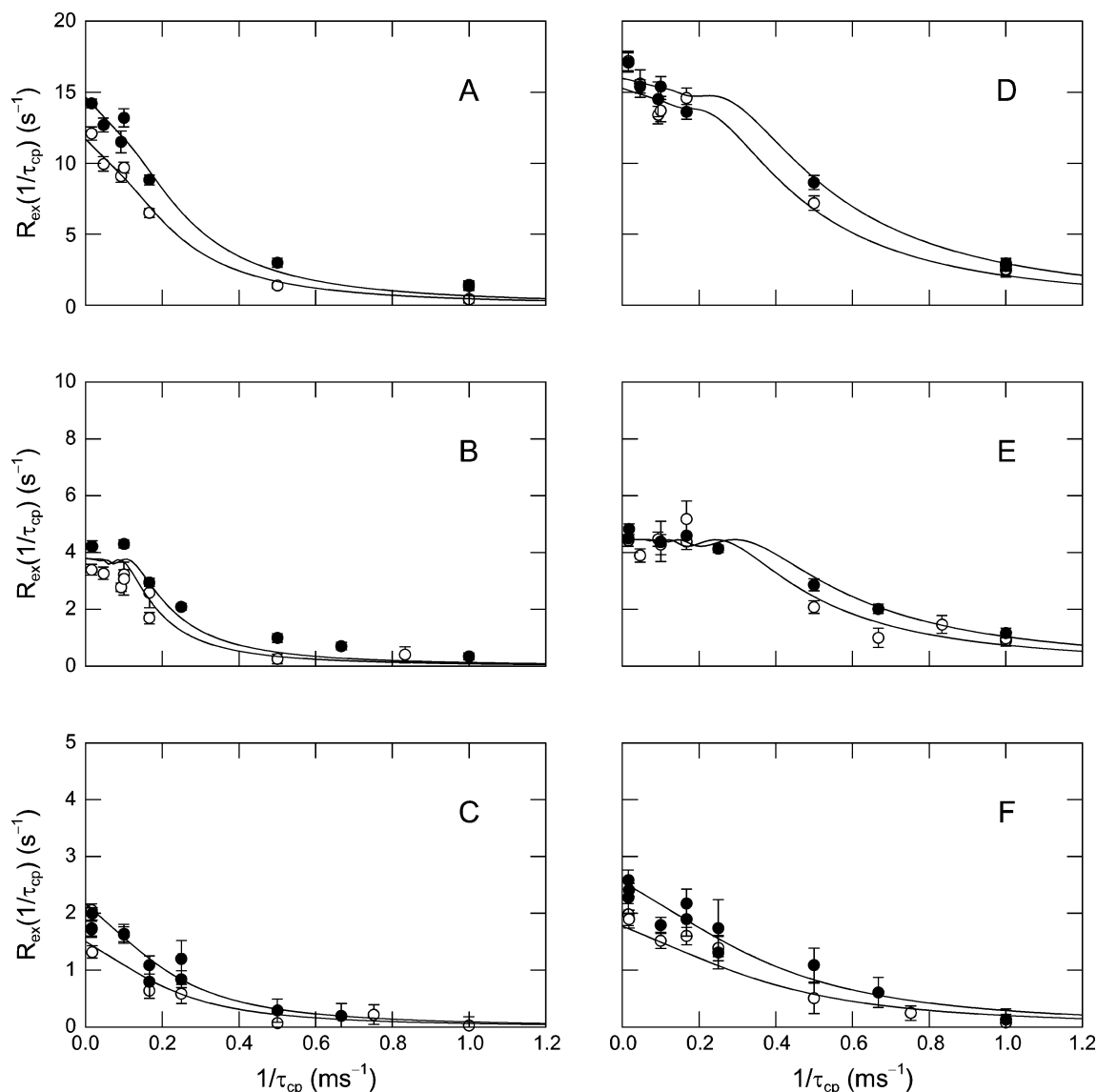**Figure 6.** Chemical exchange for C38 and R39. ^{15}N $R_{ex}(1/\tau_{cp})$ dispersion profiles for C38 (A−C) and R39 (D−F) measured at static magnetic fields of 11.7 (○) and 14.1 T (●). The solid lines represent the best simultaneous fits of the dispersion data at both fields to eq 8 at temperatures of 300 (A, D) and 290 K (B, E), or eq 10 at 280 K (C, F).
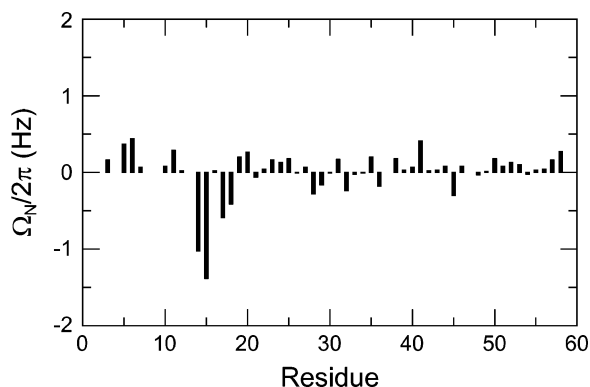

Figure 7. Sign of $\Delta\omega_N$. The difference in ^{15}N resonance frequency between ^1H−^{15}N HSQC and HMQC spectra, $\Omega_N/2\pi = \nu_N^{HSQC} - \nu_N^{HMQC}$, measured at a static magnetic field of 11.7 T and a temperature of 280 K, is plotted versus BPTI sequence.

for both of these residues. The sign of $\Delta\omega_N$ cannot be determined for C38 and R39, because, even at 280 K, exchange is too fast and Ω_N is too small.

Modeling the Minor State Conformation. The relaxation dispersion data demonstrate that exchange contributions to the ^{15}N spin relaxation of C14 and K15 in the temperature range of 280−300 K and C38 and R39 at 280 K do not result from the isomerization of the C38 side chain. To investigate the conformational change that underlies the observed exchange broadening, correlations between ^{15}N chemical shifts and conformational preferences were extracted from a database of uniformly referenced chemical shifts[43] for proteins whose structures have been determined to high resolution. For all Cys residues with backbone conformations similar to that of C14, a difference in the average secondary chemical shifts of -4 ± 5 ppm is observed for residues with $\chi_1 = +60°$ compared to $\chi_1 = -60°$ (Figure 8A), with a corresponding upfield shift for the amide nitrogen of residues immediately following Cys (Figure 8B). In addition, Figure 8C suggests that a change in χ_1 from $-60°$ to $+60°$ would be accompanied by an increase in the backbone ψ dihedral angle with a corresponding decrease of approximately -0.1 ppm degree^{-1} for the ^{15}N chemical shift

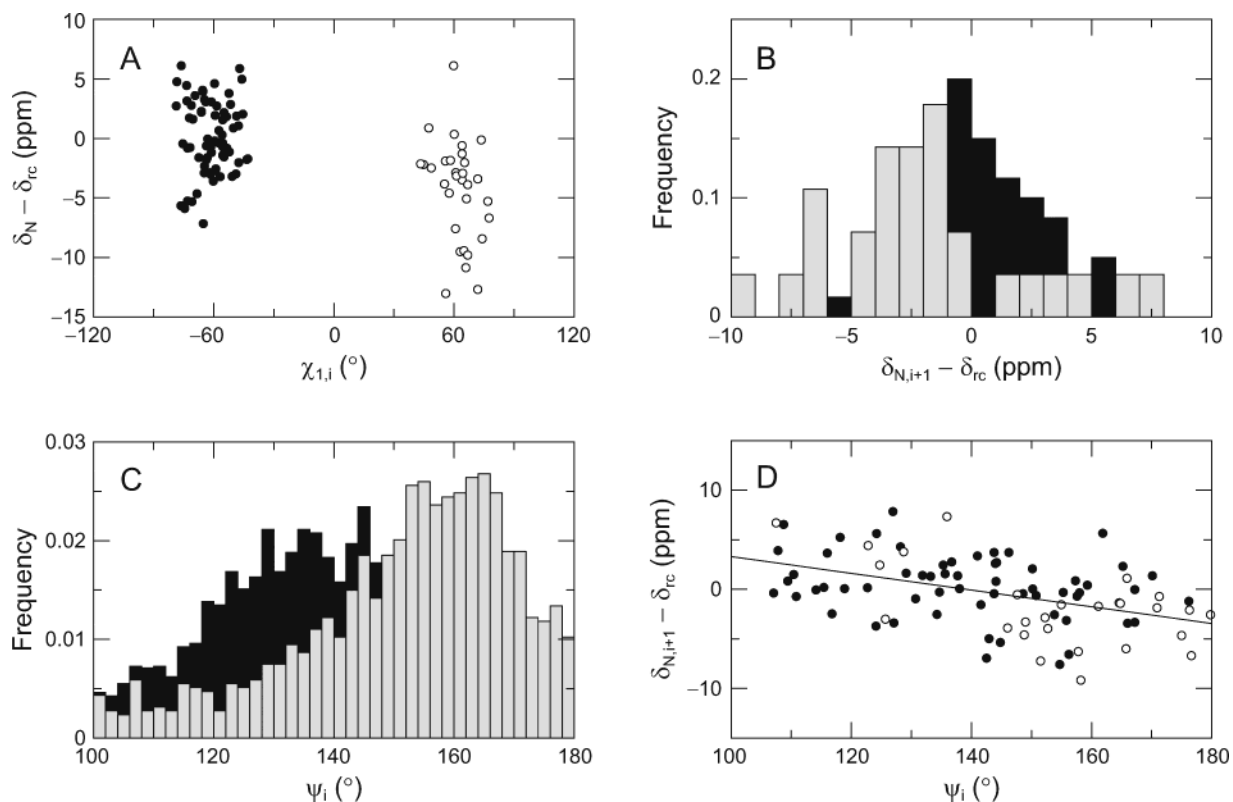**Figure 8.** χ_1 dependence of ^{15}N chemical shifts. (A) The secondary ^{15}N chemical shifts, $\delta_{N,i} - \delta_{rc}$, for the amide nitrogens of all cysteine residues, denoted residue i, with backbone $\psi_i > 100°$ and $\chi_{1,i} = -60° \pm 20°$ (●) or $\chi_{1,i} = +60° \pm 20°$ (○) from the RefDB chemical shift database[43] are plotted against χ_1 dihedral angle. The average difference in secondary chemical shift between the two rotameric states is 4 ± 5 ppm. (B) Distribution of secondary ^{15}N chemical shifts, $\delta_{N,i+1} - \delta_{rc}$, for all residues immediately following cysteine residues with $\chi_{1,i} = -60° \pm 20°$ (black bars) and $\chi_{1,i} = +60° \pm 20°$ (gray bars). (C) Distribution of backbone ψ_i dihedral angles for all residues in sheetlike conformations in the database with $\chi_{1,i} = -60° \pm 20°$ (black bars) or $\chi_{1,i} = +60° \pm 20°$ (gray bars). (D) The secondary ^{15}N chemical shifts for all residues following cysteine residues with $\chi_{1,i} = -60° \pm 20°$ (●) and $\chi_{1,i} = +60° \pm 20°$ (○) plotted versus cysteine backbone ψ_i dihedral angle. The solid line represents the least-squares fit of both data sets to a slope of -0.08 ± 0.02 ppm degree^{-1} and an intercept of 12 ± 2 ppm.

of the following residue (Figure 8D). Therefore, isomerization of the C14 χ_1 dihedral angle from $-60°$ in the major conformation to $+60°$ in the minor conformation provides a plausible mechanism for the chemical shift changes determined for C14 and K15 from the relaxation dispersion data.

To further investigate the hypothesis that C14 exists in a minor conformation characterized by a χ_1 isomerization, a model of BPTI was built in which the C14 χ_1 dihedral angle was rotated by approximately 120° from $-60°$ to $+60°$. The conformations of the C14−C38 disulfide bond in the major state (*M*) and minor states in which the χ_1 dihedrals of C14 and C38 are rotated by 120° (m_{C14}) and $-120°$ (m_{C38}), respectively, are shown in Figure 9. The effect of both isomerization reactions is to convert the geometry of the disulfide bond from right-handed in *M* to left-handed in both m_{C14} and m_{C38}. Following energy minimization of the m_{C14} model structure, the S−S dihedral, $\chi_3 = -135°$, compared to the ideal value of $-90°$ for a left-handed disulfide bond.[48,49] However, theoretical calculations indicate that the potential energy for χ_3 has a broad minimum and deviations from ideal geometry can be tolerated.[50,51] Only a small difference exists for the ψ dihedral angle of C14 between the minimized *M* and m_{C14} structures, but $\Delta\psi$ is 20° for m_{C14} compared to the unminimized crystal structure.[52] Differences in ^{15}N chemical

(48) Richardson, J. S. *Adv. Protein Chem.* **1981**, *34*, 167−339.
(49) Thornton, J. M. *J. Mol. Biol.* **1981**, *151*, 261−287.
(50) Pullman, B.; Pullman, A. *Adv. Protein Chem.* **1974**, *28*, 347−526.
(51) Jiao, D.; Barfield, M.; Combariza, J. E.; Hruby, V. J. *J. Am. Chem. Soc.* **1992**, *114*, 3639−3643.
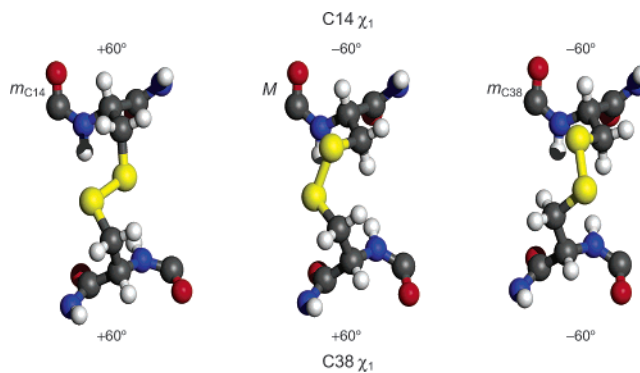

Figure 9. Conformations of the C14−C38 disulfide bond. Ball and stick representations of the C14−C38 disulfide bond in the major state (*M*), in the minor state with C14 χ_1 rotated by 120° (m_{C14}), and in the minor state with C38 χ_1 rotated by $-120°$ (m_{C38}). The models are oriented with the backbone of C14 toward the top of the figure, and they include the preceding and succeeding carbonyl and amide groups for reference. The corresponding χ_1 dihedral angles of C14 and C38 are indicated for each conformation. Atoms are colored according to: nitrogen (blue), oxygen (red), carbon (gray), hydrogen (white), and sulfur (gold).

shifts were calculated based on the minimized structures of the major and minor state structures using the semiempirical program SHIFTX.[44] The predicted shift changes, $\Delta\delta_N$, summarized in Table 4, are in agreement with both the sign and magnitude of those obtained from the relaxation dispersion

(52) Wlodawer, A.; Walter, J.; Huber, R.; Sjolin, L. *J. Mol. Biol.* **1984**, *180*, 301−329.

Table 4. Comparison of Measured and Predicted ^{15}N Chemical Shift Changes Due to the Isomerization of the C14−C38 Disulfide Bond

$\Delta\chi_1$	residue	$\Delta\delta_N^{meas}$ (ppm)	$\Delta\delta_N^{calcd}$ (ppm)
C14 ($-60° \rightarrow +60°$)	C14[a]	-3.6 ± 0.2	-3.7
	K15[a]	-4.7 ± 0.3	-1.4
	C38[b]	$\|0.84\| \pm 0.08$	-0.6
	R39[b]	$\|1.20\| \pm 0.07$	-0.4
C38 ($+60° \rightarrow -60°$)	C14[c]	0.4	-0.1
	K15[c]	0.5	0.4
	C38[c]	1.7	4.9
	R39[c]	3.7	2.3

$\Delta\delta_N^{meas} = \Delta\omega_N/|\gamma_N B_0|$ was obtained from (a) the global analysis of ^{15}N $R_{ex}(1/\tau_{cp})$ temperature dependence, (b) ^{15}N $R_{ex}(1/\tau_{cp})$ relaxation dispersion at 280 K, and (c) values reported by Otting et al.[40] Signs of $\Delta\delta_N$ in (a) were determined from the HSQC/HMQC experiment.[36]

analysis. In particular, the calculations predict the dominant effect on the ^{15}N shift of the Cys residue undergoing the χ_1 transition, as well as the secondary effect on the Cys across the disulfide bond.

Discussion

The dynamic properties of BPTI in the vicinity of the C14−C38 disulfide bond have been investigated using NMR ^{15}N spin relaxation measurements. The temperature, static magnetic field, and applied effective field dependence of exchange contributions to ^{15}N transverse relaxation have been quantified to characterize the kinetic, thermodynamic, and structural basis for chemical exchange processes affecting residues C14, K15, C38, and R39. The results indicate that at least two distinct motions occur on the microsecond−millisecond time scale in the vicinity of the disulfide bond. One process, as has been shown previously,[40] results from the interconversion of C38 χ_1 side chain rotamers, whereas the second, significantly faster, motion results from an analogous isomerization of the C14 side chain. The following sections discuss the differentiation between multiple exchange processes using relaxation dispersion measurements, the correlation of chemical shift changes with structural changes for the minor conformations, and a comparison of the kinetics and thermodynamics of the transitions between the three observed C14−C38 disulfide bond conformations.

Characterizing Chemical Exchange Dynamics from Relaxation Dispersion. Identifying the exchange process affecting the ^{15}N spins of C14 and K15 has been hampered by the lack of significant relaxation dispersion in earlier $R_{1\rho}$ and CPMG experiments.[5,41] These negative results suggested that the ^{15}N resonances of C14 and K15 were affected by a kinetic process faster than 1000 s^{-1}, but kinetic rate constants and other parameters for the exchange process could not be determined. The limitations of the previous approaches were circumvented herein by independently determining R_2^0, which constrains $R_{ex}(1/\tau_{cp} \rightarrow \infty) = 0$ and allows characterization of exchange events that are significantly faster than the strongest accessible effective field strength.[42] This is illustrated by the analysis of K15 dispersion data at 300 K, where $k_{ex} = 7400$ s$^{-1} \gg 1/\tau_{cp} = 1000$ s^{-1}.

At 300 K, both isomerization of C14 and of C38 contribute to the observed exchange line broadening for C14. Isomerization of the C38 χ_1 dihedral angle, with $k_{ex} = 580$ s^{-1}, causes a 0.4 ppm chemical shift change for the ^{15}N spin of C14, compared to the -3.6 ppm change for the C14 isomerization, with $k_{ex} = $

5500 s^{-1}. Simulated relaxation dispersion curves for C14 show that these two processes make nearly equal contributions to the experimentally observed $R_{ex}(1/\tau_{cp} \rightarrow 0)$, but with qualitatively distinct dependence on the effective field strength. Consequently, a linear three-site exchange model was required to reproduce the two distinct phases of the relaxation dispersion curve.

The relaxation dispersion data for K15 and R39, the residues immediately following C14 and C38, yield somewhat larger exchange rate constants ($\sim$35%) than reported by the two Cys residues. As a result, the dispersion curve for K15 is dominated by the faster exchange process and more closely approximates two-state behavior. This difference, which is roughly the same size as the experimental uncertainties, may indicate that additional kinetic processes remain to be discovered in BPTI. For example, the conformational fluctuations in BPTI that are presumed necessary to allow W122 to exchange with bulk solvent have yet to be identified.[39]

The results for C14 at 300 K illustrate useful points for characterizing chemical exchange between multiple sites using CPMG or $R_{1\rho}$ methods. (i) The theoretical and experimental results based on eqs 5, 13, and 15 demonstrate that multiple processes contribute to discrete phases of the relaxation dispersion profiles when $\kappa_i \gg \kappa_j$ and exchange is fast on the chemical shift time scale. These phases must be adequately defined experimentally in order to ascertain whether a two- or multisite exchange model is applicable. Independent estimates of R_2^0 aid in the detection of fast exchange processes that do not display significant relaxation dispersion because the apparent R_2 at the fastest pulsing rate or largest effective field will be greater than R_2^0. (ii) Although eq 13 provides a compact analytical expression for describing three-site chemical exchange in the fast exchange limit, site populations and chemical shift changes cannot be independently determined from ϕ_2 and ϕ_3. The same limitation exists for two-site exchange in the fast exchange limit, eq 10. This restriction is removed outside the fast exchange limit;[5] however, analytical expressions for multisite exchange on all time scales, such as eq 8 for two-site exchange, do not exist and numerical fitting of eq 1 is required.[28] (iii) In favorable cases, the three-site problem can be reduced to separate two-site reactions by using temperature to manipulate the chemical shift time scale. For processes that are in the limit of very slow or very fast exchange on the chemical shift time scale, the resulting exchange contributions to transverse relaxation are negligible. Thus, exchange broadening due to a slower process can be "frozen out" on the chemical shift time scale by lowering the sample temperature, as shown here for C38 and R39 at 280 K. Line broadening due to the faster process can be narrowed by raising the sample temperature, as shown for C38 and R39 at $T \geq 300$ K. In either case, the exchange contributions from the remaining process can be treated using theoretical expressions available for exchange between two sites. Global analysis of relaxation dispersion data recorded at multiple static magnetic fields and temperatures further enhances the reliability of curve fitting exchange models to the experimental data.

Correlating Chemical Shift Changes with Structural Changes in the Minor States. $R_{1\rho}$ and CPMG relaxation dispersion methods are becoming widely used for characterizing the kinetics and thermodynamics of functionally relevant conformational changes in proteins.[21] The chemical shift changes between major and minor species obtained from relaxation
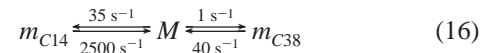
dispersion data potentially provide structural information on otherwise inaccessible conformational states. In some cases, the chemical shift changes have been interpreted using chemical shifts available for an alternative structural state of the protein, such as an apo or ligated conformation,[14,16] or using random coil chemical shifts for disordered conformations.[31,35,36] Herein, correlations observed in a chemical shift and protein structure database were used to hypothesize that the ^{15}N chemical shift changes for residues C14, K15, C38, and R39 result from a 120° isomerization of the C14 χ_1 dihedral angle. The correlation between the chemical shift changes measured by relaxation dispersion and calculated based on the proposed minor conformation validates the proposed model and illustrates the strong dependence of ^{15}N chemical shifts on local side chain conformations.[53] Chemical shift calculations suggest that an alternative structure in which the side chains of both C14 and C38 have isomerized simultaneously to give χ_1(C14, C38) = +60°, −60°, would result in ~4 ppm chemical shift changes for both C14 and C38. No evidence exists for an exchange process with large shifts changes for both residues on a common time scale. Thus, the conformation in which the side chains of both C14 and C38 have isomerized must be populated only to a very limited extent, below the limit of detection of relaxation dispersion measurements (<0.5%). The C14 and C38 χ_1 rotamer transitions appear to be largely independent, rather than highly correlated.

Isomerization of C14 as the mechanism for chemical exchange line broadening of C14 and K15 is consistent with other observations. First, the pattern of chemical shift changes observed for these residues mirror the perturbations caused by the C38 χ_1 isomerization. In both cases, large effects are observed for the Cys undergoing the isomerization and the adjacent residue and smaller effects are obtained across the disulfide bond. Second, similar chemical exchange parameters were estimated for residues in the vicinity of the C36−C45 disulfide bond in the epidermal growth factor like domain of heregulin-α.[54] This partially solvent exposed disulfide bond also adopts a right-handed conformation where χ_1 for both Cys residues is approximately −60°.[55] The static magnetic field dependence of R_2 for residues R44, C45, and T46 prompted the hypothesis that the C36−C45 disulfide bond isomerized with k_{ex} = 5000 s^{−1}, assuming chemical shift changes of 3.5 ppm and a minor state population of 5%.[54] In this case, relaxation dispersion data were not recorded. Therefore, isomerization on the microsecond−millisecond time scale appears to be an attribute of solvent-exposed disulfide bonds.

The strong dependence of ^{15}N chemical shifts on local side chain conformation was utilized here to propose and corroborate a model of the minor state conformation. Additional structural information potentially can be obtained from the effects of the exchange process on the chemical shifts of other spins by extending relaxation dispersion methods to [1]H[N,2] [13]C[α,31] and [13]CO[56] spins. In combination with database analysis,[43,57,58] quantum chemical shift calculations,[59,60] and conformational

sampling methods,[61] NMR spin relaxation dispersion provides a powerful approach for modeling structures of minor state conformations, which are otherwise invisible to conventional structural techniques.

Kinetic and Thermodynamic Comparison of the Transitions Between C14−C38 Disulfide Bond Conformations. At equilibrium, the C14−C38 disulfide bond in BPTI exists in three different conformations described by

$$m_{C14} \underset{2500 \text{ s}^{-1}}{\overset{35 \text{ s}^{-1}}{\rightleftharpoons}} M \underset{40 \text{ s}^{-1}}{\overset{1 \text{ s}^{-1}}{\rightleftharpoons}} m_{C38} \qquad (16)$$

with rate constants given for a temperature of 290 K. Inspection of the crystal structures and models of the minor state conformations suggests that isomerization of C14 or C38 would involve a transition state in which χ_3 is cis or trans with respect to the C[β] atoms, respectively. Studies on model disulfide bonded compounds indicate that the cis rotational barrier is 20−40 kJ mol^{−1} higher than that of the trans transition state for the transition from left-handed to right-handed conformations,[51] consistent with the larger $\Delta H^{\ddagger}_{-1}$ = 65 kJ mol^{−1} for the C14 isomerization compared with $\Delta H^{\ddagger}_{-1}$ = 45 kJ mol^{−1} for the C38 isomerization. However, the C14 isomerization is ultimately faster due to favorable entropic effects that reduce the transition state free energy compared to the C38 isomerization.

The primary effect of disulfide bonds in stabilizing folded protein structures is thought to arise from the reduction of configurational entropy in the unfolded state,[62,63] although numerous studies have demonstrated that disulfide bonds can significantly affect thermodynamics of the native state.[64] The unusually high thermal stability of BPTI[65] is attributed, at least in part, to the presence of three disulfide bonds. In particular, removal of the C14−C38 disulfide bond decreases the denaturation temperature by 20 K and reduces the overall stability by 35 kJ mol^{−1}.[66,67] Despite this substantial contribution to the thermodynamic stability of BPTI, the C14−C38 disulfide bond adopts a sterically unfavorable right-handed geometry. In the modeled conformation of m_{C14}, both χ_1 dihedral angles of C14 and C38 are approximately +60°, which is unusual for left-handed disulfide bonds in proteins.[48,49] This geometry has been observed, however, in single crystals of L-cysteine, where $\chi_1 \approx$ +60° and $\chi_2 \approx \chi_3 \approx$ −90°.[68] Using an empirical potential function describing the strain energy of the disulfide bond,[69] this conformation is predicted to be 2−8 kJ mol^{−1} more stable than the conformation in state M. This calculation is consistent with the slightly favorable change in enthalpy, ΔH = −7 kJ mol^{−1}, obtained for C14 and K15. However, the energetically more favorable disulfide bond geometry in m_{C14} is offset by the unfavorable entropy change, ΔS = −60 J mol^{−1} K^{−1}. In contrast, the favorable entropy change of ΔS = +20 J mol^{−1} K^{−1} associated with the m_{C38} minor state is not large enough to compensate for an unfavorable disulfide bond geometry (ΔH

(53) Wishart, D. S.; Case, D. A. *Methods Enzymol.* **2001**, *338*, 3−34.
(54) Fairbrother, W. J.; Liu, J.; Pisacane, P. I.; Sliwkowski, M. X.; Palmer, A. G. *J. Mol. Biol.* **1998**, *279*, 1149−1161.
(55) Jacobsen, N. E.; Abadi, N.; Sliwkowski, M. X.; Reilly, D.; Skelton, N. J.; Fairbrother, W. J. *Biochemistry* **1996**, *35*, 3402−3417.
(56) Mulder, F. A. A.; Akke, M. *Magn. Reson. Chem.* **2003**, *41*, 853−865.
(57) Xu, X.-P.; Case, D. A. *J. Biomol. NMR* **2001**, *21*, 321−333.
(58) Xu, X.-P.; Case, D. A. *Biopolymers* **2002**, *65*, 408−423.
(59) Sitkoff, D.; Case, D. A. *Prog. Nucl. Magn. Reson. Spectrosc.* **1998**, *32*, 165−190.

(60) Oldfield, E. *Annu. Rev. Phys. Chem.* **2002**, *53*, 349−378.
(61) Scheurer, C.; Skrynnikov, N. R.; Lienin, S. F.; Straus, S. K.; Bruschweiler, R.; Ernst, R. R. *J. Am. Chem. Soc.* **1999**, *121*, 4242−4251.
(62) Poland, D. C.; Scheraga, H. A. *Biopolymers* **1965**, *3*, 379−399.
(63) Flory, P. J. *J. Am. Chem. Soc.* **1956**, *78*, 5222−5235.
(64) Betz, S. F. *Prot. Sci.* **1993**, *2*, 1551−1558.
(65) Moses, E.; Hinz, H. J. *J. Mol. Biol.* **1983**, *170*, 765−776.
(66) Wagner, G.; Wüthrich, K. *J. Mol. Biol.* **1979**, *130*, 31−37.
(67) Schwarz, H.; Hinz, H. J.; Mehlich, A.; Tschesche, H.; Wenzel, H. R. *Biochemistry* **1987**, *26*, 3544−3551.
(68) Gupta, S. C.; Sequeira, A.; Chidambaram, R. *Acta Crystallogr. B* **1974**, *30*, 562−567.
(69) Katz, B. A.; Kossiakoff, A. *J. Biol. Chem.* **1986**, *261*, 15 480−15 485.

= +10 kJ mol^{-1}). Thus, the relative thermodynamic stabilities of the three C14−C38 disulfide bond conformations demonstrate that interactions within the native state, in addition to the local disulfide bond geometry, constrain particular conformations and consequently influence the contributions of disulfide bonds to thermodynamic stability.

Conclusions

CPMG relaxation dispersion measurements at two static magnetic fields, 11.7 and 14.1 T, and three temperatures, 280, 290, and 300 K have been used to characterize the kinetic, thermodynamic, and structural basis of chemical exchange line broadening of ^{15}N spins of C14, K15, C38, and R39 in BPTI. The results indicate that chemical exchange contributions to transverse relaxation of C14 and K15 arise from the isomerization of the C14 χ_1 dihedral angle. At 290 K, this process occurs with forward and reverse rate constants of 35 s^{-1} and 2500 s^{-1}, and the minor state conformation is populated by 1.4% of the molecules at equilibrium. The kinetics and thermodynamics of the C14 χ_1 isomerization are distinct from the independent C38 χ_1 isomerization, which occurs nearly 30-fold less frequently. The relative stabilities of the three C14−C38 disulfide bond conformations illustrate the effects of interactions in the native state on protein thermodynamics.

The analysis of the relaxation dispersion data was facilitated by the use of an analytical expression for a linear three-site exchange model to distinguish contributions from isomerization of the C14 and C38 dihedral angles, and of a global analysis of the temperature and static magnetic field dependence of $R_{ex}(1/\tau_{cp})$ to determine the activation parameters and chemical shift changes for chemical exchange line broadening of C14 and K15. The conformation of the minor state was determined by comparing chemical shift changes obtained from the relaxation dispersion analysis with both a database of chemical shifts and chemical shifts calculated from the proposed structure. Identification of this hitherto unsuspected conformational state of BPTI illustrates the utility of relaxation dispersion measurement performed at multiple static magnetic fields and temperatures for characterizing dynamic processes on microsecond–millisecond time scales in proteins. These approaches for delineating the effects of multiple exchange pathways and identifying novel conformational states advance the utility of CPMG and $R_{1\rho}$ relaxation dispersion methods to characterize the complex dynamic behavior of biological macromolecules.

Materials and Methods

NMR Spectroscopy. NMR ^{15}N spin relaxation measurements were performed on a 2.6 mM [U-98% ^{15}N] labeled BPTI sample in 90% H$_2$O, 10% D$_2$O at pH 5.1. Data were collected at static magnetic field strengths of 11.7 and 14.1 T using Bruker DRX500 and DRX600 spectrometers equipped with triple-resonance three-axis gradient probes. Sample temperatures of 280, 290, and 300 K were calibrated by measuring the difference between the hydroxyl and methyl proton resonance frequencies of a 100% methanol sample. All data sets were collected and processed as described previously,[42] with postacquisition processing performed using the NMRPipe software package.[70] ^{1}H–^{15}N cross-peak assignments were taken from Glushka et al.,[71] and the peak volumes were integrated using nlinLS.[70] All ^{15}N spin relaxation

rate constants were determined using the nonlinear least-squares fitting routine implemented by the in-house program CurveFit (available from www.palmer.hs.columbia.edu), with uncertainties estimated by jackknife simulations.[72]

$R_{ex}(1/\tau_{cp})$ Relaxation Dispersion. ^{15}N $R_2^{rczz}(1/\tau_{cp})$ spin relaxation rate constants were measured using rczz CPMG pulse sequences as described previously[42] for the following values of τ_{cp} (ms) at each temperature and static field: (300 K, 11.7 T) 1.0 (2×), 2.0, 6.0, 10.0, 10.8, 21.6, 64.8; (300 K, 14.1 T) 1.0 (3×), 2.0, 6.0, 10.0, 10.8, 21.6, 64.8; (290 K, 11.7 T) 1.0 (2×), 1.5, 2.0, 6.0, 10.0 (2×), 10.8, 21.6, 64.8; (290 K, 14.1 T) 1.0, 1.5, 2.0, 4.0, 6.0, 10.0, 57.9, 64.8; (280 K, 11.7 T) 1.0, 1.3, 2.0, 4.0, 6.0, 10.0, 10.8, 64.8; (280 K, 14.1 T) 1.0, 1.5, 2.0, 4.0 (2×), 6.0 (2×), 10.0, 10.8, 21.6, 57.9, 64.8. For $\tau_{cp} =$ 57.9 ms, a Hahn spin–echo pulse sequence employing WALTZ16 ^{1}H decoupling during the relaxation period[73,74] was used to acquire four spectra with $t = 0$ ms and four spectra with $t = 2\tau_{cp}$. The apparent relaxation rate constant, R_2^{echo}, was determined from the single-exponential decay of the relative peak volumes, and $R_2^{rczz}(1/\tau_{cp} = 17.3$ s$^{-1}) = R_2^{echo} − R_1/2$.

^{15}N spin–lattice (R_1), spin–spin (R_2),[75] and ^{1}H−^{15}N dipolar/^{15}N CSA transverse cross-correlated (η_{xy})[76] relaxation rate constants were measured as described previously to determine $R_2^{0,rczz}$.[42] The limiting relaxation rate constant in the rczz CPMG experiments is given by $R_2^{0,rczz} = \eta_{xy}/\Gamma − R_1/2$, where $\Gamma = (\eta_{xy}/R_2^0)$. An average value of Γ was determined from the weighted least squares slope of a plot of η_{xy} versus R_2, excluding data for exchanging residues G12, C14, K15, A16, R17, I18, G36, C38, R39, A40, and K41. The uncertainty in $R_2^{0,rczz}$ was estimated by propagating the experimental error in η_{xy}, Γ, and R_1. $R_{ex}(1/\tau_{cp})$ was calculated for each value of τ_{cp} from

$$R_{ex}(1/\tau_{cp}) = R_2^{rczz}(1/\tau_{cp}) − R_2^{0,rczz} \qquad (17)$$

with the uncertainties estimated by propagating the experimental errors in each rate constants. Analyses of the $R_{ex}(1/\tau_{cp})$ relaxation dispersion data at a single temperature and multiple static magnetic field strengths were performed by fitting the data with eqs 4, 8, 10, and 13 as appropriate. Global analyses of $R_{ex}(1/\tau_{cp})$ relaxation dispersion data at multiple temperatures and multiple static magnetic field strengths were performed using eqs 8 and 11, assuming that $\Delta\omega_N$ was independent of temperature. The Levenberg−Marquardt algorithm was used for nonlinear least squares optimization.[77] Fitting was performed with the in-house program CPMGFit (available from www.palmer.hs.columbia. edu) or routines written in Mathematica 4.2 (Wolfram Research). Uncertainties in the optimized exchange parameters were estimated from jackknife simulations.[72]

HSQC and HMQC Correlation Spectra. The HSQC/HMQC method[36] was used to determine the sign of $\Delta\omega_N$ obtained from the fitting of $R_{ex}(1/\tau_{cp})$ dispersion data. Pulse sequences from HSQC and HMQC experiments were used as described previously,[36] with the exception that the HMQC experiment was modified to have the same number of pulses as the HSQC experiment to minimize differences in sample heating between the two experiments. The spectra were acquired at 11.7 T and 280 K, and processed in the same manner as the spin relaxation experiments. After processing, duplicate frequency domain spectra were added to increase the overall signal-to-noise ratio. The

(70) Delaglio, F.; Grzesiek, S.; Vuister, G. W.; Zhu, G.; Pfeifer, J.; Bax, A. *J. Biomol. NMR* **1995**, *6*, 277−293.
(71) Glushka, J.; Lee, M.; Coffin, S.; Cowburn, D. *J. Am. Chem. Soc.* **1989**, *111*, 7716−7722.

(72) Mosteller, F.; Tukey, J. W. *Data Analysis and Regression: A Second Course in Statistics*; Addison-Wesley Publishing Company: Reading, Massachusetts, 1977.
(73) Wang, L.; Pang, Y.; Holder, T.; Brender, J. R.; Kurochkin, A. V.; Zuiderweg, E. R. P. *Proc. Natl. Acad. Sci. U.S.A.* **2001**, *98*, 7684−7689.
(74) Wang, C.; Palmer, A. G. *Magn. Reson. Chem.* **2003**, *41*, 866−876.
(75) Farrow, N. A.; Muhandiram, R.; Singer, A. U.; Pascal, S. M.; Kay, C. M.; Gish, G.; Shoelson, S. E.; Pawson, T.; Forman-Kay, J. D.; Kay, L. E. *Biochemistry* **1994**, *33*, 5984−6003.
(76) Kroenke, C. D.; Loria, J. P.; Lee, L. K.; Rance, M.; Palmer, A. G. *J. Am. Chem. Soc.* **1998**, *120*, 7905−7915.
(77) Press, W. H.; Flannery, B. P.; Teukolsky, S. A.; Vetterling, W. T. *Numerical Recipes. The Art of Scientific Computing*; Cambridge University Press: Cambridge, 1986.

differences in peak positions were calculated as $\Omega_N/2\pi = \nu_N^{\text{HSQC}} - \nu_N^{\text{HMQC}}$, where $\nu_N^{\text{H(S/M)QC}}$ is the frequency of the peak in the ^{15}N dimension of the HSQC and HMQC experiments.

Structural Modeling of the Minor Conformations. A database of ^{15}N chemical shifts for all proteins with structures determined to high resolution (<2 Å) was constructed from the RefDB database of uniformly referenced protein chemical shifts.[43] For each residue in the database, the secondary chemical shift was calculated as $\delta_N - \delta_{\text{rc}}$, where δ_N is the observed chemical shift in the RefDB and δ_{rc} is the sequence-corrected random coil chemical shift.[78] Backbone dihedral angles ϕ and ψ, and side chain dihedral angles χ_1 and χ_2 were calculated based on the atomic coordinates from the corresponding PDB entry.

Structural models of the minor exchange conformations were generated based on the atomic coordinates of BPTI, crystal form II, using the proton positions determined from the joint refinement of X-ray and neutron scattering data.[52] Any undetermined proton coordinates were constructed using the HBUILD module of CHARMM.[79] The minor conformations of the C14−C38 disulfide bond were constructed by rotation of the side chain atoms of C14 or C38 by 120° and −120°, respectively, about the axis defined by the C_α and C_β atoms. For all three structures (one major and two minor conformations), the protein was solvated in an octahedron shell of TIP3 water molecules. The system was subjected to 200 steps of steepest descent minimization followed by conjugate gradient energy minimization until the change in energy converged to less than 0.2 kJ mol^{-1}. Constraints were

employed only on the proton atoms using the SHAKE algorithm and the CHARMM22 all-atom potential force field[80] was utilized. The quality of the minimized structures was validated using PROCHECK,[81] which did not report any significant structural violations. After energy minimization the disulfide dihedral angles (C14 − χ_1, χ_2, χ_3, χ_2, χ_1 − C38) were: (*M*) −60°, 101°, 90°, −130°, 74°; (m_{C14}) 50°, −110°, −135°, −70°, 66°; (m_{C38}) −68°, 150°, −90°, 130°, −48°. ^{15}N chemical shifts were calculated for the energy-minimized structures using the program SHIFTX,[44] and the chemical shift change was determined as $\Delta\delta_N = \delta_N^{\text{minor}} - \delta_N^{\text{major}}$.

(78) Braun, D.; Wider, G.; Wüthrich, K. *J. Am. Chem. Soc.* **1994**, *116*, 8466−8469.
(79) Brooks, B. R.; Bruccoleri, R. E.; Olafson, B. D.; States, D. J.; Swaminathan, S.; Karplus, M. *J. Comput. Chem.* **1983**, *4*, 187−217.
(80) MacKerell, A. D., Jr.; Bashford, D.; Bellott, M.; Dunbrack, R. L.; Evanseck, J. D.; Field, M. J.; Fischer, S.; Gao, J.; Guo, H.; Ha, S.; Joseph-McCarthy, D.; Kuchnir, L.; Kuczera, K.; Lau, F. T. K.; Mattos, C.; Michnick, S.; Ngo, T.; Nguyen, D. T.; Prodhom, B.; Reiher, W. E., III; Roux, B.; Schlenkrich, M.; Smith, J. C.; Stote, R.; Straub, J.; Watanabe, M.; Wiorkiewicz-Kuczera, J.; Yin, D.; Karplus, M. *J. Phys. Chem. B* **1998**, *102*, 3586−3616.
(81) Laskowski, R. A.; Macarthur, M. W.; Moss, D. S.; Thornton, J. M. *J. Appl. Crystallogr.* **1993**, *26*, 283−291.
(82) Koradi, R.; Billeter, M.; Wüthrich, K. *J. Mol. Graph.* **1996**, *14*, 51−55, plates, 29−32.